Electronic Supplementary Information

Heterometallic Molecular Ni-Salen Catalysts for Efficient Electrocatalytic Oxygen Evolution Reaction

Kiran Bhadauriya,[a] Ayusie Goyal,[a] Rakesh Kumar,[a] Baghendra Singh,[a]* Apparao Draksharapu,[a]*

[a]Southern Laboratories - 208A, Department of Chemistry, Indian Institute of Technology Kanpur, Kanpur-208016 (India).

E-mail: baghendras@iitk.ac.in, appud@iitk.ac.in

EXPERIMENTAL SECTION

Materials and Methods

All chemicals and reagents used in the present study that are commercially available were used as received. All metal salts *e.g.* $NiCl_2.6H_2O$, $Mn(ClO_4)_2.6H_2O$, $Co(ClO_4)_2.6H_2O$ and $Fe(ClO_4)_2.6H_2O$ were purchased from Sigma-Aldrich. While *o*-vanillin and *(1R, 2R)*-cyclohexane-1,2-diamine were purchased from BLD pharma. HPLC grade dry acetonitrile from Thomas Baker were used in the spectroscopic studies. Diethyl ether was purchased from Qualigens. Nickel foam was procured from D-Tech Solutions, Kanpur, India. Double distilled water was used for electrochemical testing.

Instruments

UV-Vis absorption spectroscopic studies were performed by Agilent 8453 diode-array spectrophotometer to carry out kinetics experiments spectrophotometrically in 1 cm quartz cells (λ = 190-1100 nm range). Fourier transform infrared (FT-IR) spectra were acquired in attenuated total reflectance (ATR) mode. Surface chemical states were examined by X-ray photoelectron spectroscopy (XPS) on a PHI 5000 Versa Probe III model. XPS data fitting was carried out using Origin Pro 2022b software.

Diffraction intensities were collected on a Bruker SMART APEX CCD diffractometer, with graphite-monochromated Mo K_α (0.71073 Å) radiation at 100(2) K. Data were corrected for Lorentz and polarization effects; empirical absorption corrections (SADABS-2016/2 (Bruker,2016/2)) was used for absorption correction were applied. The structures were solved by SHELXT and refined with the SHELXL package incorporated into the Olex2-1.5 crystallographic collective package. All non-hydrogen atoms were refined with anisotropic thermal parameters using full-matrix least-squares procedures on F2. CCDC 2502530 – 2502532 contains the supplementary crystallographic data for compound **2**-**4** respectively. This data can be acquired via http://www.ccdc.cam.ac.uk or from the Cambridge Crystallographic Data Centre, 12, Union Road, Cambridge CB2 1EZ, U.K.; Fax: +44 1223 336033.

Electrochemical Measurements

All the electrochemical measurements were conducted in a three-electrode system, where the metal complex (drop casted on Nickel foam) served as working electrode, Pt wire as counter electrode and non-aqueous Hg/HgO as reference electrode, with aqueous 1.0 M KOH as electrolyte. CV and linear sweep voltammetry (LSV) measurements were corrected

for 100% iR drop. The electrode potentials were converted to the reversible hydrogen electrode (RHE) scale using the formula:

$$E_{(RHE)} = E_{(Hg/HgO)} + 0.098 + 0.059\ pH$$

Electrochemical impedance spectroscopy (EIS) was performed over a frequency range of 0.01-10,00,000 Hz with an amplitude of 10 mV. The charge transfer resistance (R_{ct}) was derived from the semicircle diameter in the Nyquist plots. Chronoamperometric (CA) measurement was carried out in a 1.0 M KOH solution at a constant potential and presented without iR compensation. The Tafel slope was calculated from LSV curves (with iR compensation) at potential corresponding to fixed current density.

Activation of Nickel Foam (NF)

Nickel foam (NF) pieces measuring 1 cm × 2 cm were initially cleaned with acetone and thoroughly washed with double distilled water. The cleaned NF pieces were then sonicated in 1.0 M HCl for 10 min, rinsed again with distilled water, and dried in an oven at 50 °C for 12 h.

Synthesis of 1

Complex **1** was synthesized by following the reported procedure for the Ni-salen complex with subtle modifications.[1] Salen-OCH_3 (**L**) was synthesized by the reaction of *o*-valine (2 equiv.) with *(1R, 2R)*-cyclohexane-1,2-diamine (1 equiv.) in an ethanolic solution under reflux conditions for two hours. A yellow crystalline material was obtained after evaporating the solvent under reduced pressure. In a 50 mL round-bottom flask, 50 mg (0.13 mmoles) ligand (yellow) was dissolved in 5 mL of acetonitrile solution and mixed with 31 mg (0.13 mmoles) $NiCl_2.6H_2O$ (green) solution in acetonitrile, upon which the solution turned turbid. The reaction was stirred for 4 hours at room temperature. The solvent was evaporated under vacuum to yield a brown solid, which was washed three times with 20 mL of diethyl ether and then dried. Needle-shaped dark brown crystals of **1** were collected after recrystallization at 273 K by dissolving 10 mg of **1** in 2 mL dichloromethane under ether vapour diffusion. These crystals were directly used for the synthesis of heterometallic complexes.

Synthesis of 2, 3, and 4

Complexes **2**-**4** were synthesized by the addition of 1 equivalent of Mn^{II}/Co^{II}/Fe^{II} perchlorate salts to an acetonitrile solution of **1**, respectively. Instantly, the brown solution of **1** turned to a clear red color. These complexes were crystallized in an acetonitrile solution under ether

vapour diffusion. The red needle-shaped crystals of **2**, light-red needle-shaped crystals of **3**, and orangish-red needle-shaped crystals of **4** were obtained in a week.

Immobilization of complexes on NF[2-3]

The complexes were dissolved in acetonitrile solution to form a homogeneous solution. The solution was drop casted on 1 cm^2 surface area of activated nickel foam. The drop casted nickel foam pieces were dried at 50 ^oC for 30 minutes and further used for electrochemical evaluations.

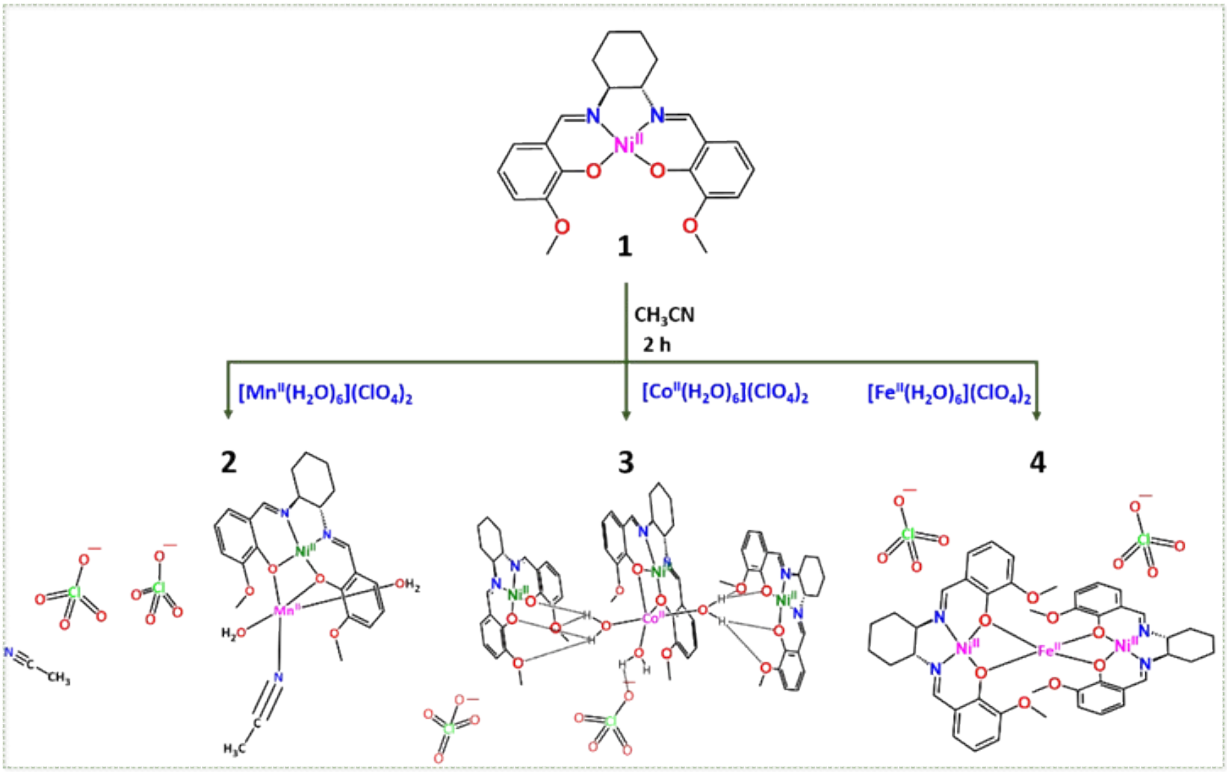

Figure S1. Synthesis scheme for the complexes **2**, **3** and **4** from **1**.

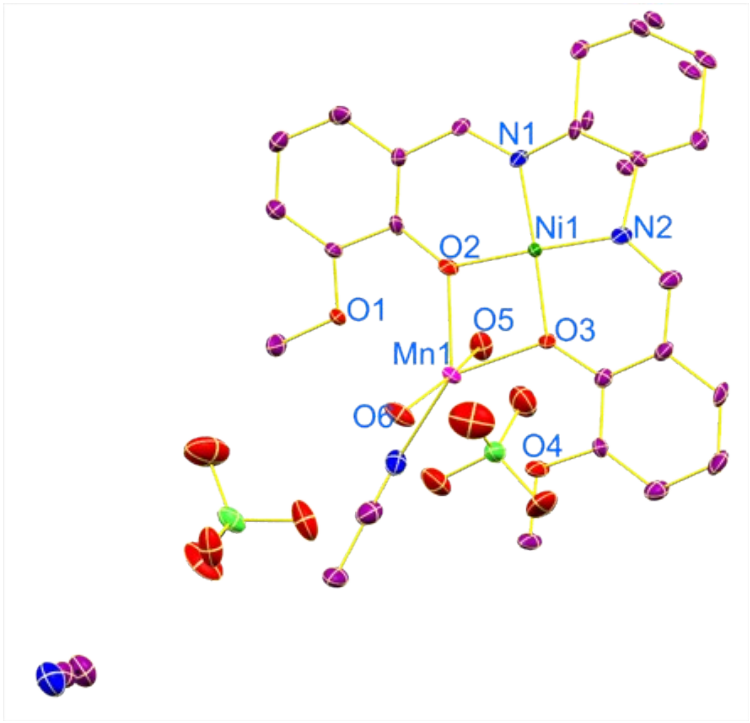

Figure S2. XRD structure of **2** collected at 100 K. Thermal ellipsoids are drawn at the 50% probability level. Hydrogen atoms are omitted for clarity.

Table S1. Crystal data and structure refinements for **2**, **3**, and **4**.

Identification code	**2**	**3**	**4**
Empirical formula	$C_{26}H_{34}Cl_2MnN_4NiO_{14}$	$C_{66}H_{78}Cl_2CoN_6Ni_3O_{23}$	$C_{44}H_{47}Cl_2FeN_4Ni_2O_{16}$
Formula weight	811.12	1629.30	1132.02
Temperature/K	100(2)	100(2)	100(2)
Crystal system	triclinic	triclinic	monoclinic
Space group	*P-1*	*P-1*	*C2*
a/Å	8.4801(13)	12.1492(4)	18.000(3)
b/Å	13.367(2)	15.5959(5)	20.400(3)
c/Å	16.142(3)	18.6011(6)	12.978(2)
α/°	100.569(4)	89.4570(10)	90
β/°	104.558(5)	78.4030(10)	108.789(6)
γ/°	105.991(4)	76.5410(10)	90
Volume/Å^3	1638.5(4)	3355.15(19)	4511.8(12)
Z	2	2	4
ρ_{calc}g/cm^3	1.644	1.613	1.667
μ/mm^{-1}	1.196	1.237	1.340
F(000)	834.0	1690.0	2332.0
Crystal size/mm^3	0.22 × 0.18 × 0.18	0.2 × 0.19 × 0.19	0.23 × 0.2 × 0.2
Radiation	MoK*α* (*λ* = 0.71073)	MoK*α* (*λ* = 0.71073)	MoK*α* (*λ* = 0.71073)
2Θ range for data collection/°	5.1 to 56.948	4.174 to 56.826	4.862 to 56.668
Index ranges	-11 ≤ *h* ≤ 11, -17 ≤ *k* ≤ 17, -21 ≤ *l* ≤ 21	-16 ≤ *h* ≤ 16, -20 ≤ *k* ≤ 20, -24 ≤ *l* ≤ 24	-23 ≤ *h* ≤ 23, -27 ≤ *k* ≤ 27, -17 ≤ *l* ≤ 17
Reflections collected	31963	95121	34175
Independent reflections	8181 [R_{int} = 0.0662, R_{sigma} = 0.0607]	16812 [R_{int} = 0.0632, R_{sigma} = 0.0445]	11223 [R_{int} = 0.0523, R_{sigma} = 0.0567]
Data/restraints/parameters	8181/12/441	16812/0/1045	11223/1/630
Goodness-of-fit on F^2	1.233	1.270	1.034
Final R indexes [I>=2σ(I)]	R_1 = 0.1256, wR_2 = 0.2839	R_1 = 0.0782, wR_2 = 0.1723	R_1 = 0.0457, wR_2 = 0.1009
Final R indexes [all data]	R_1 = 0.1339, wR_2 = 0.2877	R_1 = 0.0867, wR_2 = 0.1756	R_1 = 0.0745, wR_2 = 0.1197
Largest diff. peak/hole / *e* Å^{-3}	2.60/-2.06	1.02/-1.24	0.89/-0.71
Flack parameter	–	–	0.05(3)

Table S2. Selected Bond lengths (Å) for **2**.

		Length/Å				**Length/Å**
Ni(1)	O(3)	1.840(5)		Mn(1)	O(2)	2.200(6)
Ni(1)	O(2)	1.854(6)		Mn(1)	O(5)	2.117(6)
Ni(1)	N(1)	1.842(7)		Mn(1)	O(1)	2.527(6)
Ni(1)	N(2)	1.834(7)		Mn(1)	O(6)	2.124(7)
Mn(1)	O(3)	2.176(6)		Mn(1)	N(3)	2.279(8)
Mn(1)	O(4)	2.504(7)				

Table S3. Selected Bond angles for **2**.

			Angle/˚					**Angle/˚**
O(3)	Ni(1)	O(2)	82.2(2)		O(5)	Mn(1)	O(3)	94.1(2)
O(3)	Ni(1)	N(1)	177.3(3)		O(5)	Mn(1)	O(4)	98.9(3)
N(1)	Ni(1)	O(2)	95.1(3)		O(5)	Mn(1)	O(2)	90.6(3)
N(2)	Ni(1)	O(3)	96.0(3)		O(5)	Mn(1)	O(1)	88.2(2)
N(2)	Ni(1)	O(2)	178.1(3)		O(5)	Mn(1)	O(6)	165.2(3)
N(2)	Ni(1)	N(1)	86.7(3)		O(5)	Mn(1)	N(3)	84.9(3)
O(3)	Mn(1)	O(4)	65.8(2)		O(6)	Mn(1)	O(3)	100.7(2)
O(3)	Mn(1)	O(2)	67.4(2)		O(6)	Mn(1)	O(4)	86.2(3)
O(3)	Mn(1)	O(1)	132.9(2)		O(6)	Mn(1)	O(2)	96.0(3)
O(3)	Mn(1)	N(3)	146.0(2)		O(6)	Mn(1)	O(1)	82.6(3)
O(4)	Mn(1)	O(1)	159.8(2)		O(6)	Mn(1)	N(3)	82.2(3)
O(2)	Mn(1)	O(4)	132.7(2)		N(3)	Mn(1)	O(4)	80.7(2)
O(2)	Mn(1)	O(1)	65.5(2)		N(3)	Mn(1)	O(1)	81.1(2)
O(2)	Mn(1)	N(3)	146.4(3)		Ni(1)	O(3)	Mn(1)	105.9(3)

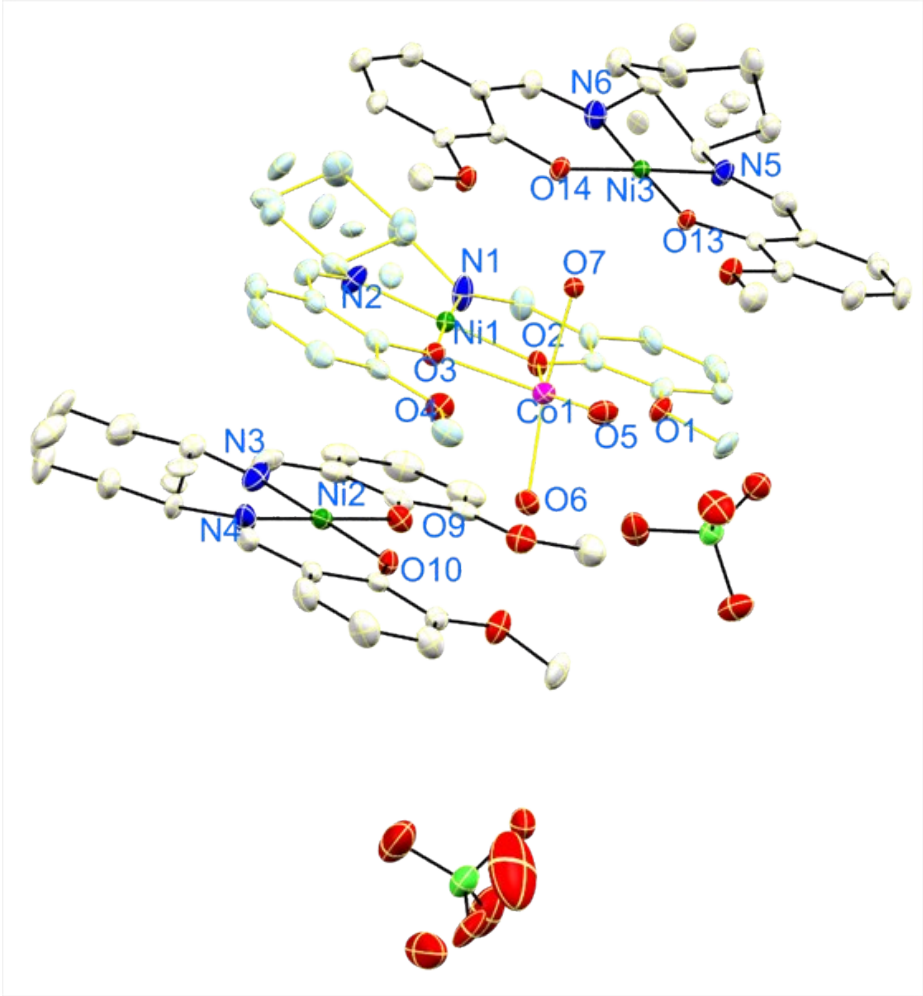

Figure S3. XRD structure of **3** collected at 100 K. Thermal ellipsoids are drawn at the 50% probability level. Hydrogen atoms are omitted for clarity.

Table S4. Selected Bond lengths (Å) for **3**.

		Length/Å				Length/Å
Ni(1)	O(2)	1.844(3)		Ni(3)	O(14)	1.846(4)
Ni(1)	O(3)	1.852(3)		Ni(3)	N(6)	1.863(4)
Ni(1)	N(1)	1.841(5)		Ni(3)	N(5)	1.849(4)
Ni(1)	N(2)	1.839(4)		Co(1)	O(2)	2.097(3)
Ni(2)	O(10)	1.839(4)		Co(1)	O(7)	2.061(3)
Ni(2)	O(9)	1.851(4)		Co(1)	O(3)	2.179(4)
Ni(2)	N(4)	1.865(5)		Co(1)	O(6)	2.050(4)
Ni(2)	N(3)	1.846(5)		Co(1)	O(1)	2.399(4)
Ni(3)	O(13)	1.858(3)		Co(1)	O(5)	2.048(4)

Table S5. Selected Bond angles for **3**.

			Angle/˚					Angle/˚
O(2)	Ni(1)	O(3)	81.25(15)		N(3)	Ni(2)	N(4)	87.0(2)
N(1)	Ni(1)	O(2)	95.45(18)		O(2)	Co(1)	O(3)	68.47(13)
N(1)	Ni(1)	O(3)	176.64(19)		O(2)	Co(1)	O(1)	69.22(12)
N(2)	Ni(1)	O(2)	177.68(18)		O(7)	Co(1)	O(2)	92.07(14)
N(2)	Ni(1)	O(3)	96.85(18)		O(7)	Co(1)	O(3)	90.38(14)
N(2)	Ni(1)	N(1)	86.5(2)		O(7)	Co(1)	O(1)	90.38(13)
O(13)	Ni(3)	N(6)	177.20(19)		O(3)	Co(1)	O(1)	137.68(12)
O(14)	Ni(3)	O(13)	84.81(15)		O(6)	Co(1)	O(2)	93.17(14)
O(14)	Ni(3)	N(6)	94.46(18)		O(6)	Co(1)	O(7)	171.58(14)
O(14)	Ni(3)	N(5)	178.52(18)		O(6)	Co(1)	O(3)	97.68(14)
N(5)	Ni(3)	O(13)	94.22(17)		O(6)	Co(1)	O(1)	85.32(14)
N(5)	Ni(3)	N(6)	86.56(19)		O(5)	Co(1)	O(2)	151.49(15)
O(10)	Ni(2)	O(9)	84.21(16)		O(5)	Co(1)	O(7)	78.44(15)
O(10)	Ni(2)	N(4)	94.20(18)		O(5)	Co(1)	O(3)	137.45(15)
O(10)	Ni(2)	N(3)	178.36(19)		O(5)	Co(1)	O(6)	93.88(15)
O(9)	Ni(2)	N(4)	178.22(19)		O(5)	Co(1)	O(1)	83.88(14)
N(3)	Ni(2)	O(9)	94.65(19)					

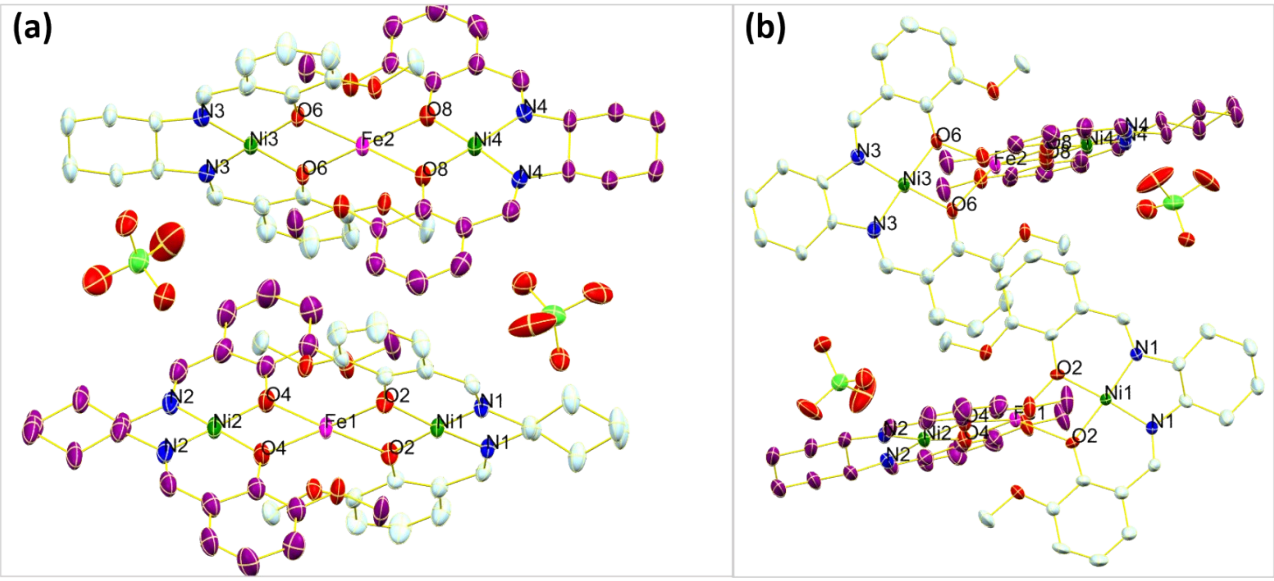

Figure S4. XRD structure of **4** collected at 100 K; (a) top view, and (b) side view. Thermal ellipsoids are drawn at the 50% probability level. Hydrogen atoms are omitted for clarity.

Table S6. Selected bond lengths (Å) for **4**.

		Length/Å				Length/Å
Ni(1)	O(2)^2	1.840(6)		Ni(4)	O(8)^1	1.830(7)
Ni(1)	O(2)	1.840(6)		Ni(4)	O(8)	1.830(7)
Ni(1)	N(1)	1.852(7)		Ni(4)	N(4)^1	1.847(8)
Ni(1)	N(1)^2	1.852(7)		Ni(4)	N(4)	1.847(8)
Ni(2)	O(4)^2	1.842(7)		Fe(1)	O(2)^2	2.099(6)
Ni(2)	O(4)	1.842(7)		Fe(1)	O(2)	2.099(6)
Ni(2)	N(2)^2	1.826(9)		Fe(1)	O(4)^2	2.112(7)
Ni(2)	N(2)	1.826(9)		Fe(1)	O(4)	2.112(7)
Ni(3)	O(6)	1.845(6)		Fe(2)	O(6)	2.133(6)
Ni(3)	O(6)^1	1.845(6)		Fe(2)	O(6)^1	2.133(6)
Ni(3)	N(3)	1.827(8)		Fe(2)	O(8)	2.127(7)
Ni(3)	N(3)^1	1.827(8)		Fe(2)	O(8)^1	2.127(7)

Table S7. Selected bond angles for **4**.

			Angle/˚					Angle/˚
O(6)	Ni(3)	O(6)^1	81.4(4)		O(2)^2	Ni(1)	N(1)^2	96.6(3)
N(3)^1	Ni(3)	O(6)	176.0(3)		O(2)^2	Ni(1)	N(1)	171.2(3)
N(3)	Ni(3)	O(6)	95.7(3)		O(2)	Ni(1)	N(1)	96.6(3)
N(3)^1	Ni(3)	O(6)^1	95.7(3)		N(1)^2	Ni(1)	N(1)	88.1(4)
N(3)	Ni(3)	O(6)^1	176.0(3)		O(4)	Ni(2)	O(4)^2	80.2(4)
N(3)^1	Ni(3)	N(3)	87.2(5)		N(2)^2	Ni(2)	O(4)^2	96.3(3)
O(6)^1	Fe(2)	O(6)	68.7(3)		N(2)^2	Ni(2)	O(4)	174.3(3)
O(8)^1	Fe(2)	O(6)^1	134.1(2)		N(2)	Ni(2)	O(4)^2	174.3(3)
O(8)^1	Fe(2)	O(6)	132.9(2)		N(2)	Ni(2)	O(4)	96.3(3)
O(8)	Fe(2)	O(6)^1	132.9(2)		N(2)^2	Ni(2)	N(2)	87.6(6)
O(8)	Fe(2)	O(6)	134.1(2)		O(2)^2	Fe(1)	O(2)	68.2(3)
O(8)^1	Fe(2)	O(8)	67.1(4)		O(2)	Fe(1)	O(4)	138.7(2)
O(8)	Ni(4)	O(8)^1	79.9(4)		O(2)	Fe(1)	O(4)^2	128.2(2)
O(8)^1	Ni(4)	N(4)	176.3(4)		O(2)^2	Fe(1)	O(4)	128.2(2)
O(8)	Ni(4)	N(4)^1	176.3(4)		O(2)^2	Fe(1)	O(4)^2	138.7(2)
O(8)	Ni(4)	N(4)	96.5(3)		O(4)^2	Fe(1)	O(4)	68.4(4)
O(8)^1	Ni(4)	N(4)^1	96.5(3)		Ni(1)	O(2)	Fe(1)	106.1(2)
N(4)^1	Ni(4)	N(4)	87.2(5)		Ni(3)	O(6)	Fe(2)	104.9(3)
O(2)	Ni(1)	O(2)^2	79.6(3)		Ni(4)	O(8)	Fe(2)	106.5(3)
O(2)	Ni(1)	N(1)^2	171.2(3)					

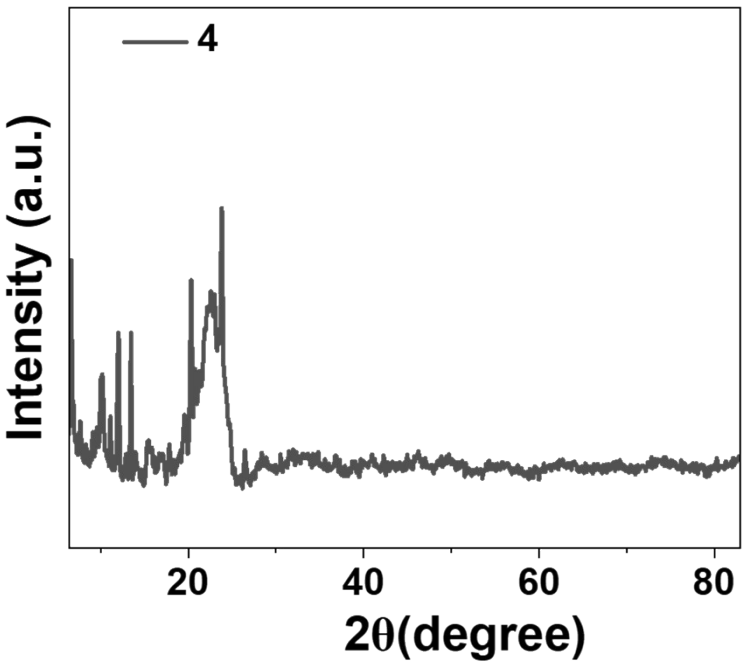

Figure S5. PXRD pattern of crude bulk material of **4**.

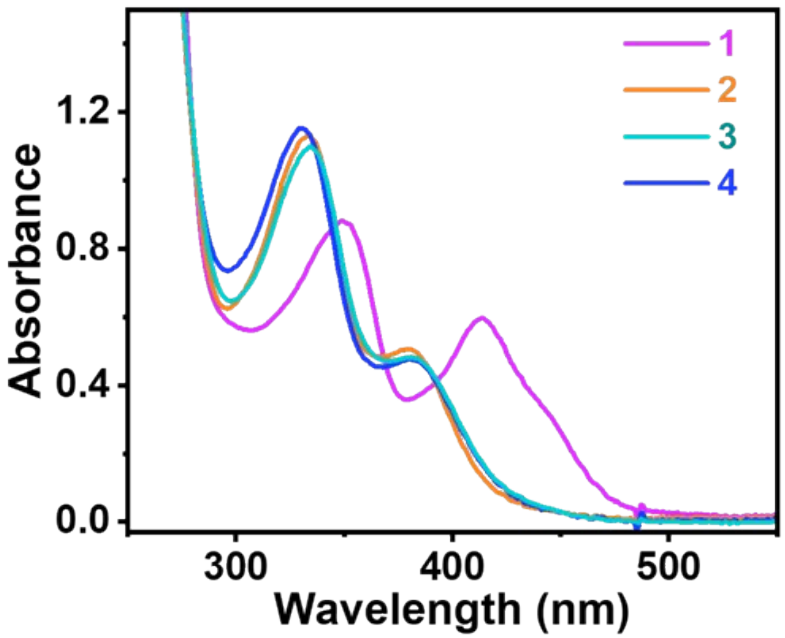

Figure S6. UV-vis absorption spectra of complexes **1**-4 (0.1 mM) were recorded in acetonitrile at room temperature.

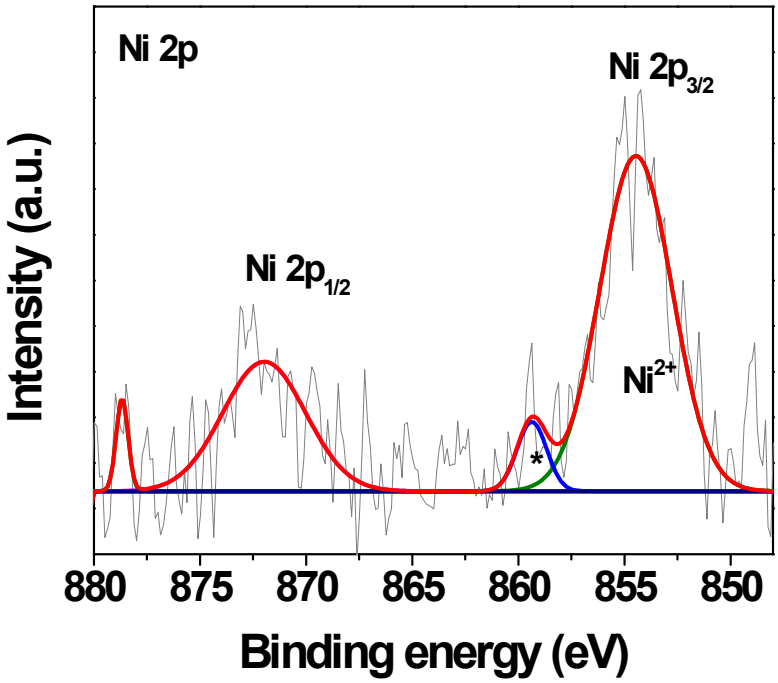

Figure S7. Ni 2p XPS data of **4** showing the signals for Ni $2p_{3/2}$ and Ni $2p_{1/2}$. The signal at 854.43 eV corresponded to Ni^{II} while * marked peaks were assigned for the satellite peaks. The Ni^{II} signal showed a positive shift of 0.80 eV compared to **1**.[4-5]

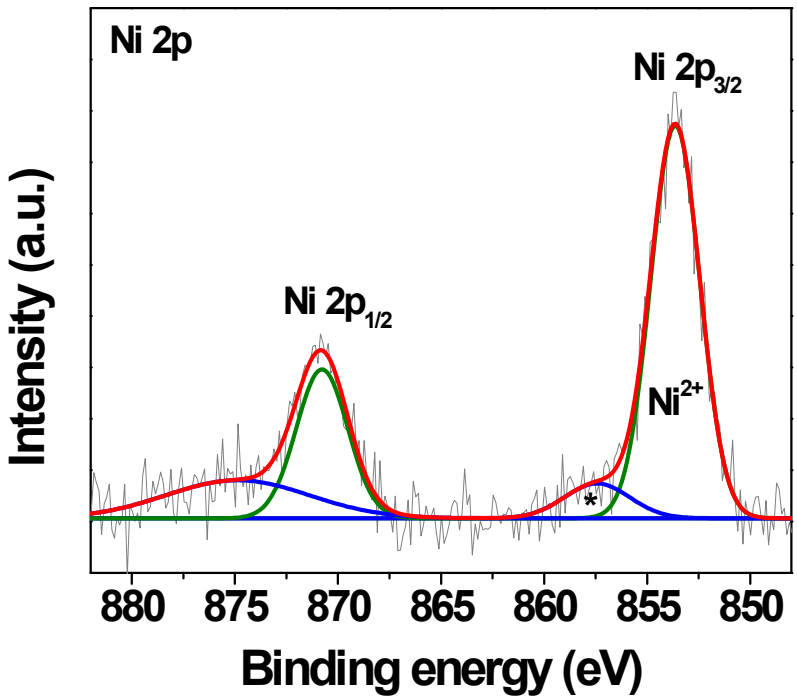

Figure S8. Ni 2p XPS data of **1** showing the signals for Ni $2p_{3/2}$ and Ni $2p_{1/2}$. The signal at 853.63 eV corresponded to Ni^{II} while * marked peaks were assigned for the satellite peaks.[4,5]

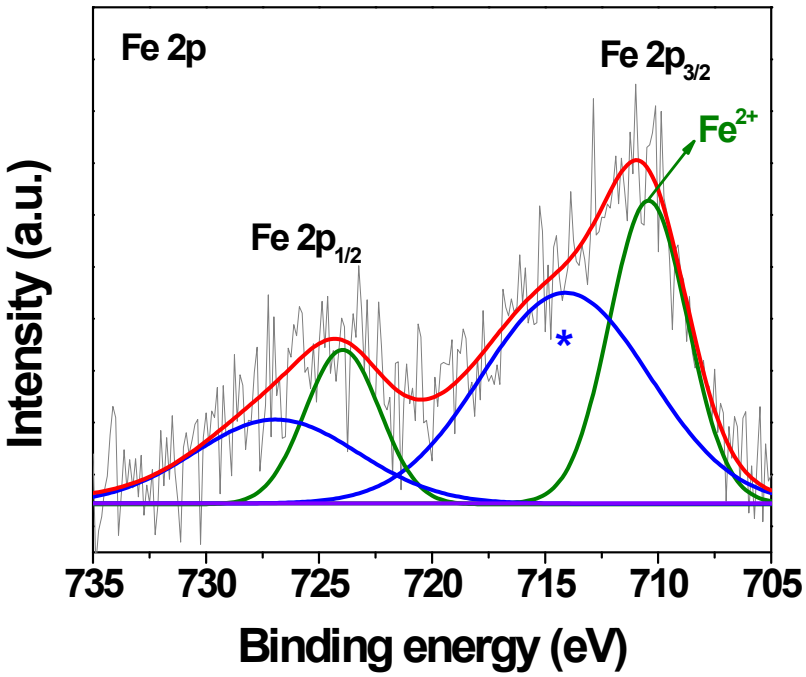

Figure S9. Fe 2p spectrum of **4**. The spectrum exhibits peak at 710.47 eV, suggesting the presence of Fe^{II} (* marked peaks are assigned for satellite peaks).[6-7]

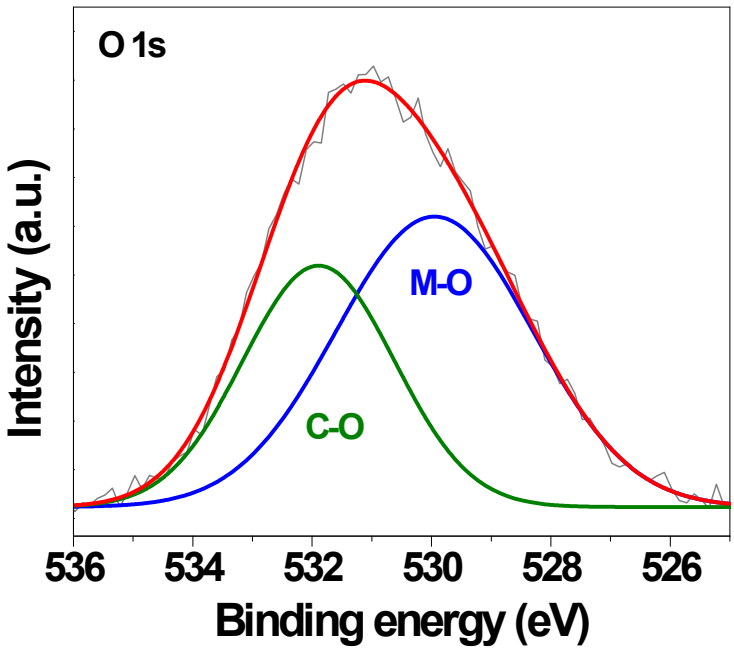

Figure S10. O 1s XPS spectrum of **1**. The spectrum displays two distinct peaks at 529.95 eV and 531.85 eV, attributed to the M–O and C-O bonds, respectively.[8-9]

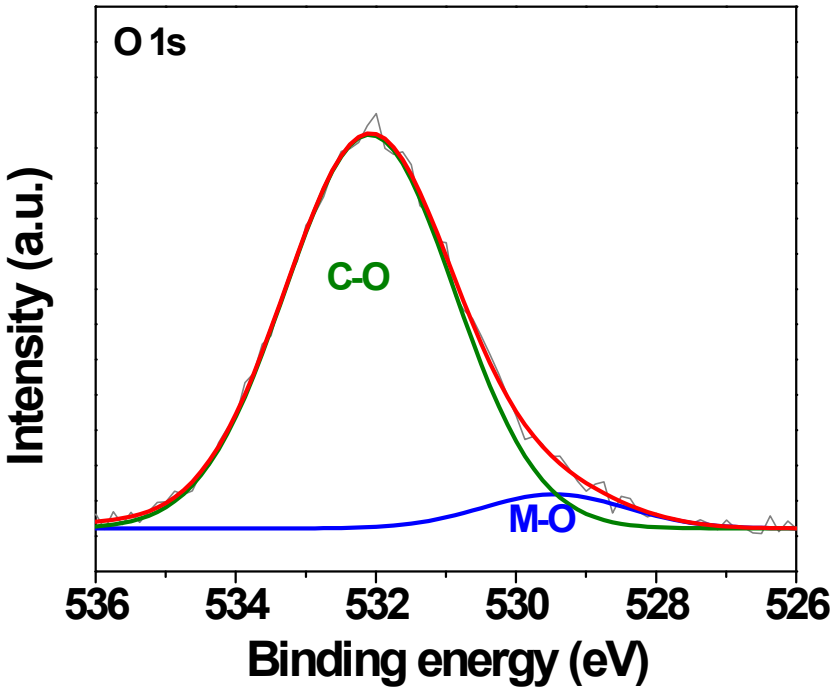

Figure S11. O 1s XPS spectrum of **4**. The spectrum displays two distinct peaks at 529.49 eV and 532.07 eV, attributed to the M–O and C-O bonds, respectively. The M-O peaks showed negative shift of 0.46 eV compared to **1**.[8-9]

Table S8. A literature survey table comparing the OER performance of related Ni(II)-based molecular catalysts.[a]

Catalyst	Electrolyte	Overpotential (mV)	Stability (h)	Reference
$[Ni(TMC)(CH_3CN)](NO_3)_2$	Phosphate buffer	590 mV @0.5 mA cm^{-2}	4	*10*
Ni–Hmfchce	0.1 KOH	490 mV @10 mA cm^{-2}	-	*11*
Ni(II)1,1-dithiolatephosphine	1.0 M KOH	350 mV @10 mA cm^{-2}	-	*12*
Ni-MOG	0.1 M KOH	418 mV @10 mA cm^{-2}	2.5	*13*
$LaNiO_{2.9}F_{0.1}$	1.0 M KOH	320 mV @10 mA cm^{-2}	-	*14*
α-$Ni(OH)_2$	0.1 M KOH	331 mV @10 mA cm^{-2}	-	15
$Ni^{II}(L_x)_2]$	1.0 M KOH	330 mV @10 mA cm^{-2}	2	*16*
$[Ni_2^{II}(dtbh\text{-}PLY)_2]$	1.0 M KOH	300 mV @10 mA cm^{-2}	10	17
$[Ni^{II}(Hmbhce)_2(py)_2]$	1.0 M KOH	328 mV @10 mA cm^{-2}	-	18
$[Ni^{II}\{(SePiPr_2)_2N\}_2]$	1.0 M KOH	200 mV @10 mA cm^{-2}	12	19
$Ni_4(LH)_4(MeOH)]\cdot CHCl_3$	1.0 M KOH	330 mV @10 mA cm^{-2}	24	20
4	**1.0 M KOH**	**350 mV @50 mA cm^{-2}**	**24**	**This work**

[a]IUPAC names/abbrebiations:

TMC[10] = 1,4,8,11-Tetramethyl-1,4,8,11-tetraazacyclotetradecane; H_2mfchce[11] = N′-(2-methylfuran-3-carbonyl)hydrazine]-carbodithioic acid ethyl ester; MOG[13] = metal organic gels; L_2[16] = *N*-methylthiophene-*N*-4-pyridylmethyl dithiocarbamate; dtbh-$PLYH_2$[17] = 9-(2-(3,6-di-*tert*-butyl-2-hydroxybenzylidene)hydrazineyl)-1*H*-phenalen-1-one; H_2mbhce[18] = N'-(4-Methyl-benzoyl)hydrazinecarbodithioic acid ethyl ester; L[20] = 2-{(*E*)-(2-hydroxyphenylimino)methyl)-6-(hydroxymethyl)-4-methylphenol}

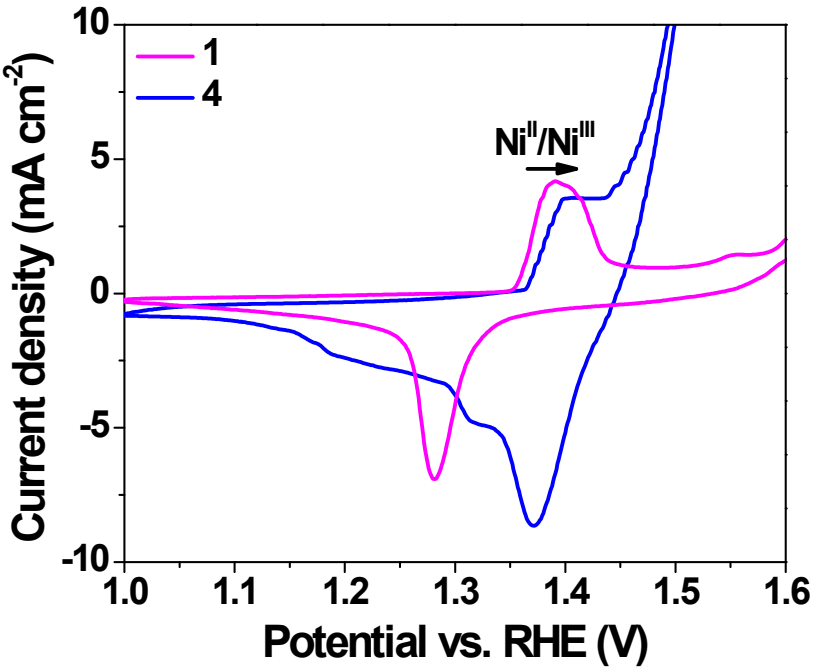

Figure S12. Cyclic voltammograms of **1** and **4**, showing the shift of Ni^{II}/Ni^{III} redox peak in **4**.[21]

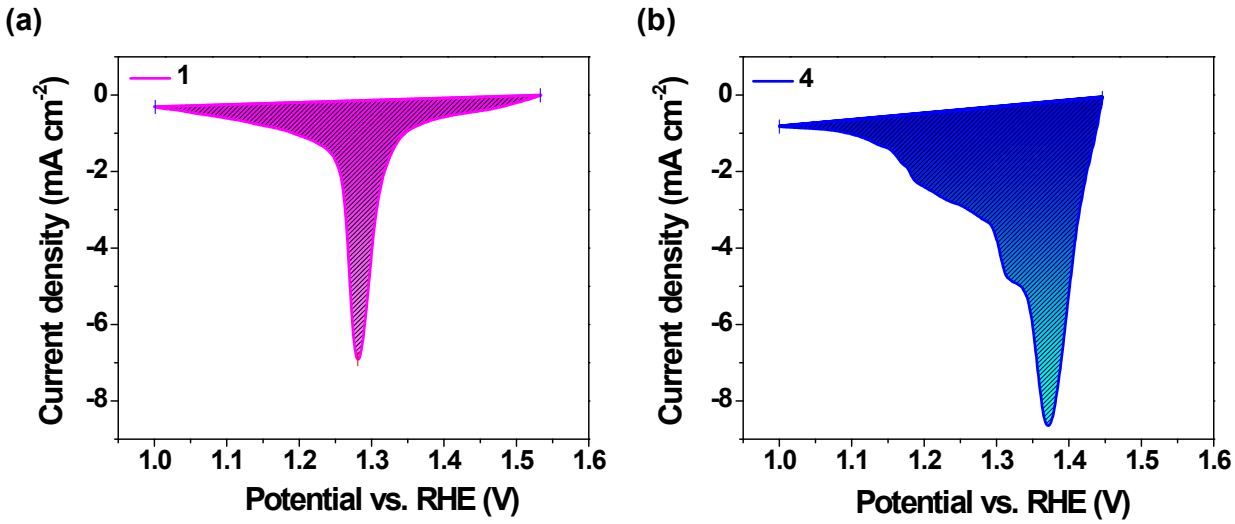

Figure S13. Reduction peak area utilized for integration to determine the number of active sites of (a) **1**, and (b) **4**.[22]

Determination of surface-active Ni-sites[22]

For **1**

Calculated area associated with the reduction peak = 0.51811×10^{-3} V A

Hence the associated charge is = 0.518×10^{-3} V A / 0.005 V s^{-1}

= 1036×10^{-4} A s

= 1036×10^{-4} C

Now, the number of electron transferred is = 1036×10^{-4} C / 1.62×10^{-19} C

= 6.39×10^{17}

Since the oxidation of Ni^{2+} to Ni^{3+} is a single electron transfer reaction, the number of electrons calculated above is the same as the number of surface-active sites.

Hence, the surface-active Ni^{3+} sites are = 6.39×10^{17}

For **4**

Calculated area associated with the reduction peak = 1.07357×10^{-3} V A

Hence the associated charge is = 1.073×10^{-3} V A / 0.005 V s^{-1}

= 2146×10^{-4} A s

= 2146×10^{-4} C

Now, the number of electron transferred is = 2146×10^{-4} C / 1.62×10^{-19} C

= 13.24×10^{17}

The surface-active Ni^{3+} sites are = 13.24×10^{17}

Calculation of Turn Over Frequency (TOF)[22]

TOF = $(j \times N_A) / (4 \times F \times n)$

where,

j = current density at η = 350 mV

N_A = Avogadro number

F = Faraday constant

n = number of active Ni-sites

For complex **4**

TOF = $[(50.0 \times 10^{-3}) (6.023 \times 10^{23})] / [(96485) (4) (13.24 \times 10^{17})]$

TOF = 5.89×10^{-2} s^{-1}

For complex **1**

TOF = $[(3.306 \times 10^{-3}) (6.023 \times 10^{23})] / [(96485) (4) (6.39 \times 10^{17})]$

TOF = 0.08×10^{-2} s^{-1}

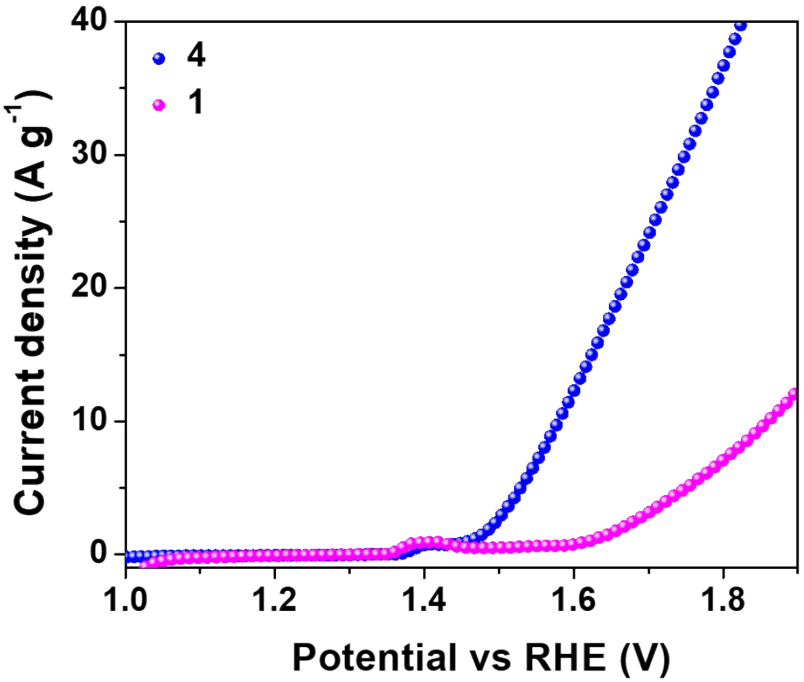

Figure S14. LSV curves of **4** and **1** normalized with mass loading.

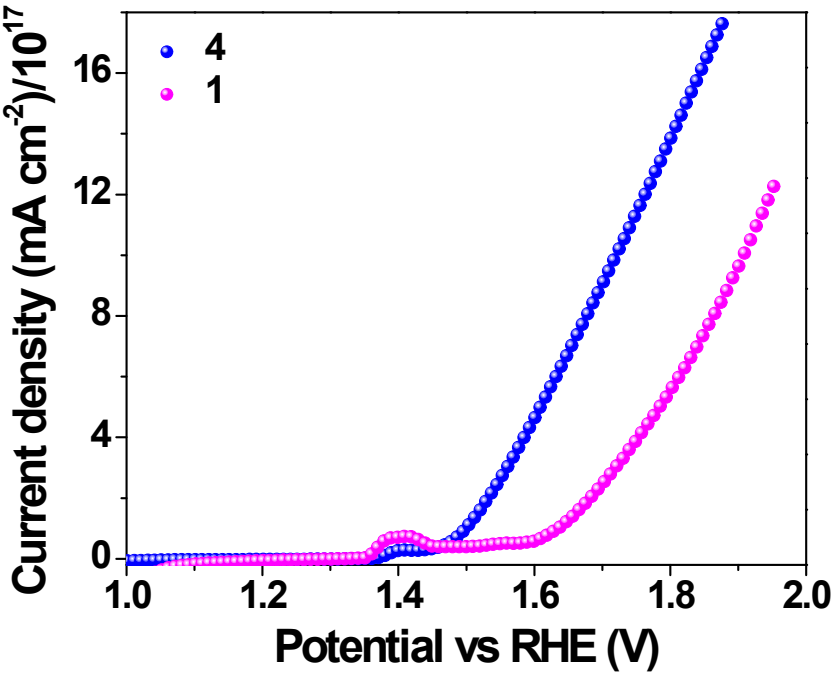

Figure S15. LSV curves of **4** and **1** normalized with number of active sites.

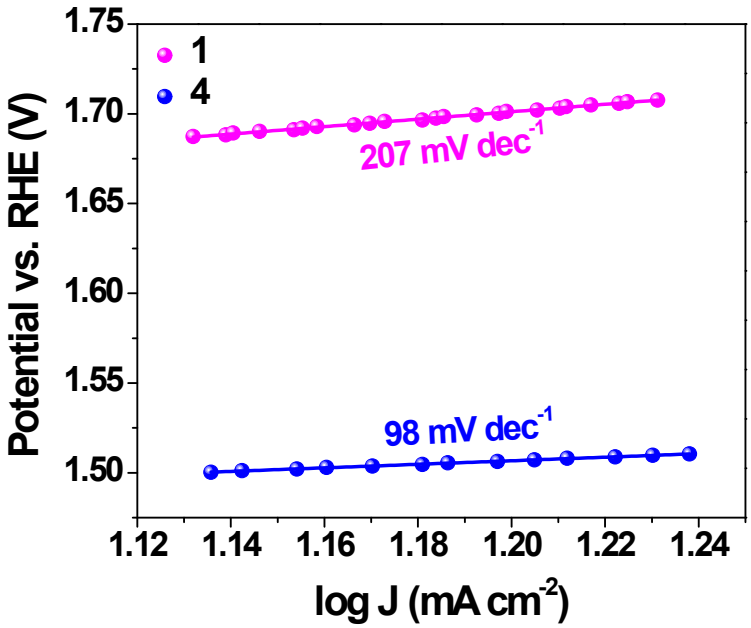

Figure S16. Tafel plots of **1** and **4**, showing a lower slope value for **4**.

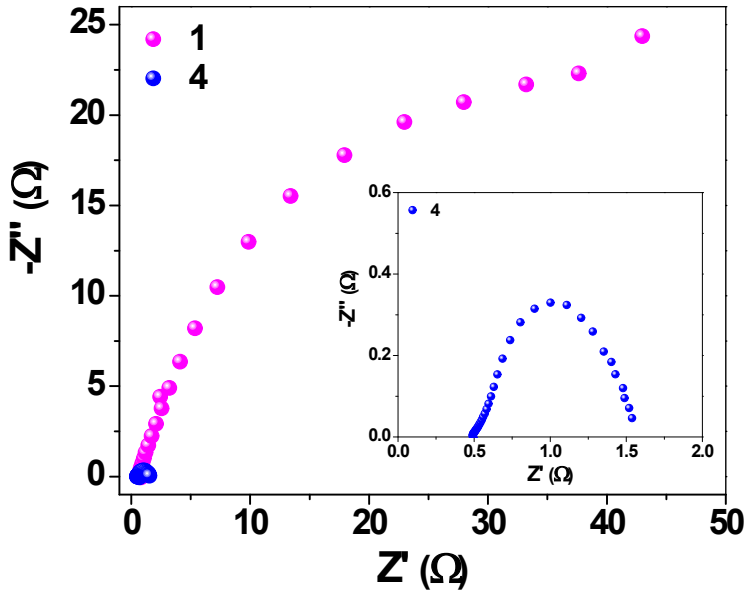

Figure S17. Nyquist plot of **1** and **4** at a potential of 1.50 V vs RHE, showing a lower semicircle radius for **4**.

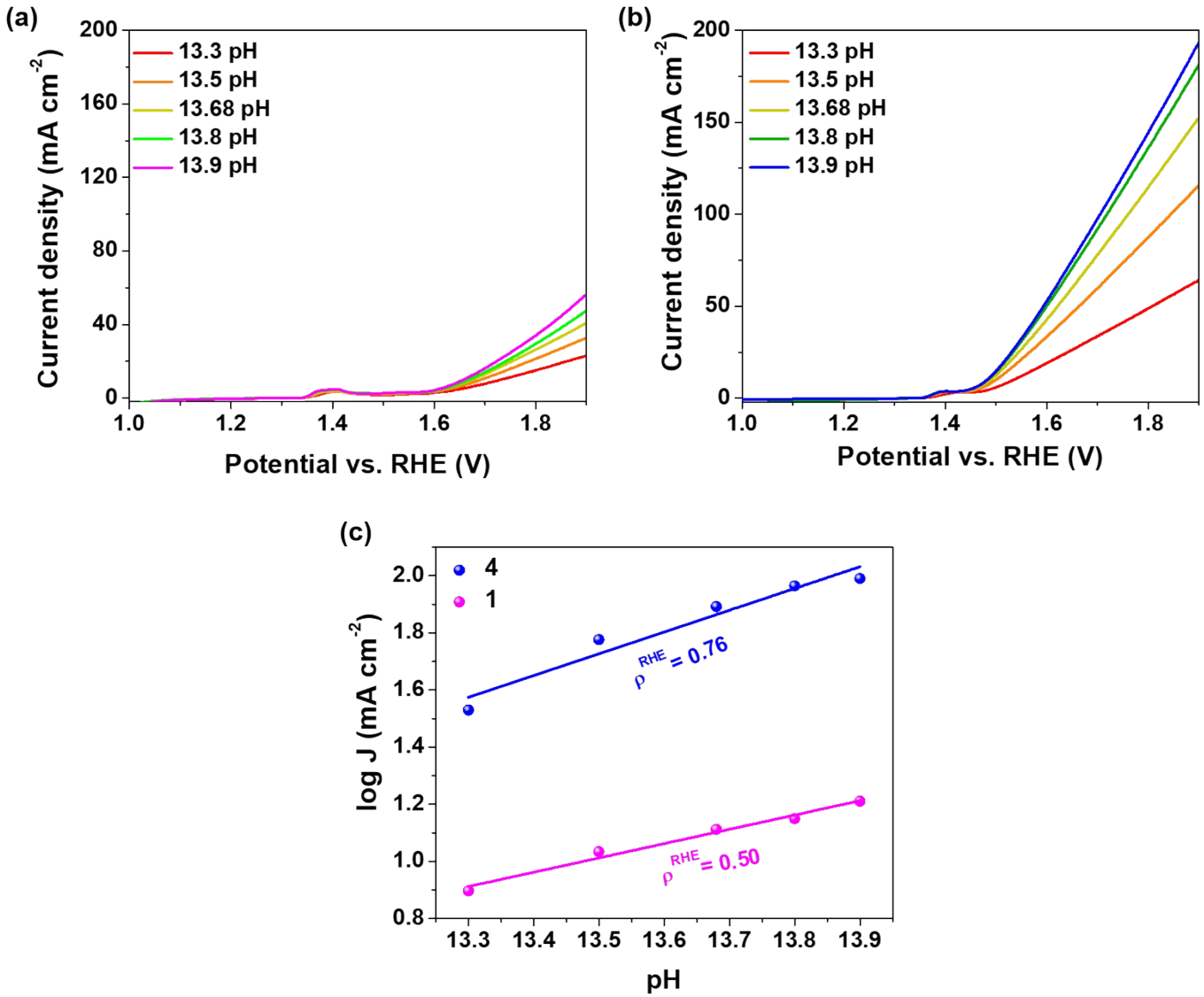

Figure S18. (a) pH-dependent OER activity of **1**, (b) pH-dependent OER activity of **4**, and (c) plot of log of current density (J) determined at 1.70 V vs. RHE against pH for **1** and **4** (without iR compensation).[23]

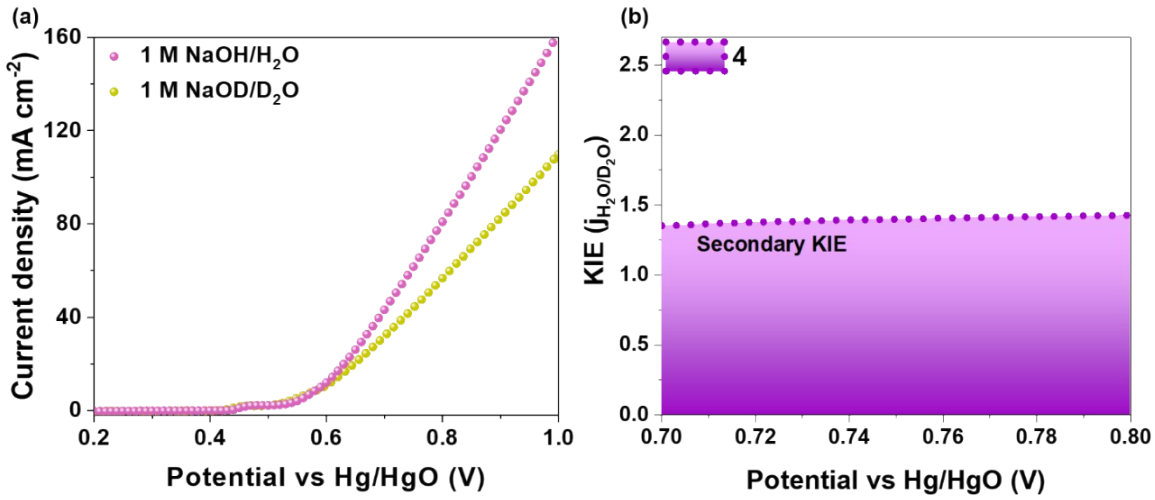

Figure S19. (a) OER-LSV profiles of **4** in 1.0 M NaOH in H_2O and 1.0 M NaOD in D_2O; and

(b) Kinetic isotope effect (KIE) studies by comparing OER current density of **4** in 1.0 M NaOH in H_2O and 1.0 M NaOD in D_2O in the potential range of 0.7-0.8 V vs Hg/HgO.[23]

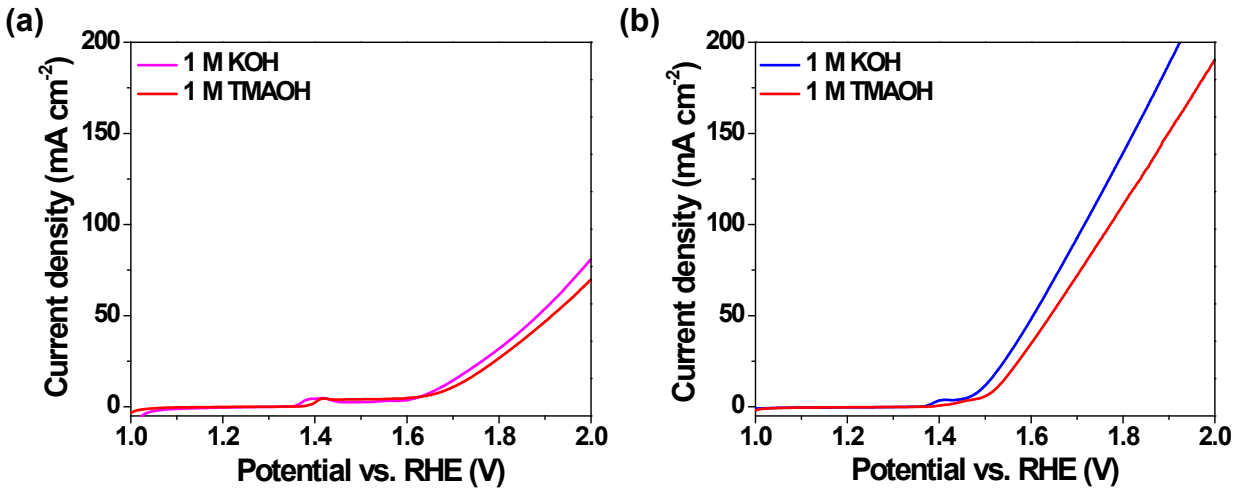

Figure S20. (a) OER activity of **1** in 1 M KOH and 1 M TMAOH, and (b) OER activity of **4** in 1 M KOH and 1 M TMAOH (without iR compensation).[24]

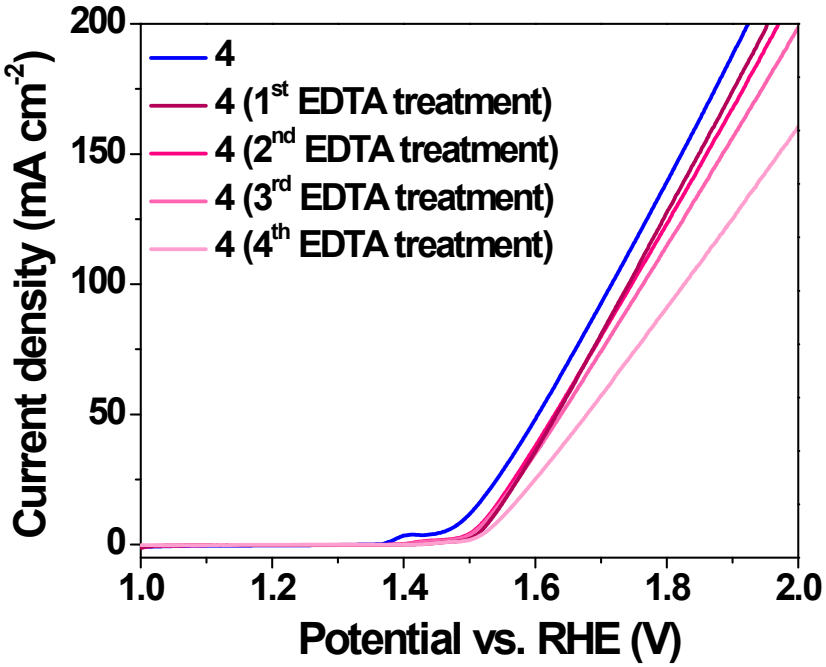

Figure S21. Change in OER activity of **4** after four successive EDTA treatments (without iR compensation).[25]

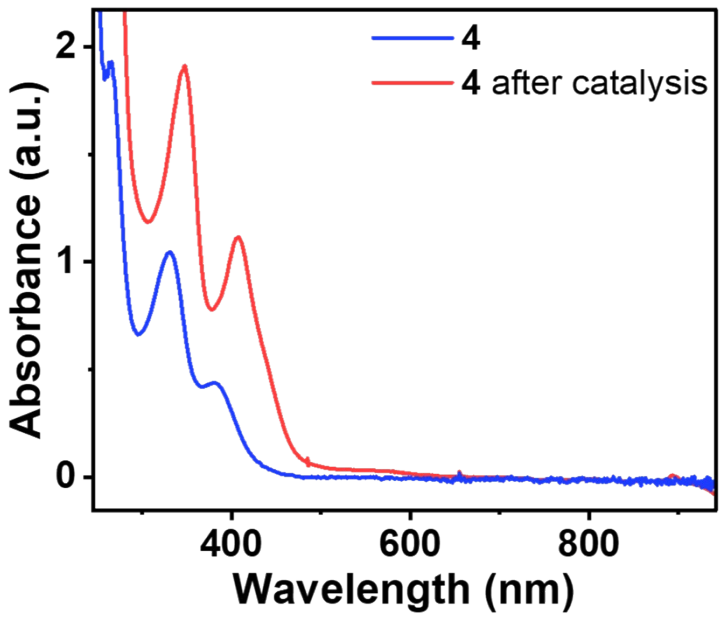

Figure S22. UV-vis absorption spectra of **4** before (blue line) and after (red line) OER catalysis.

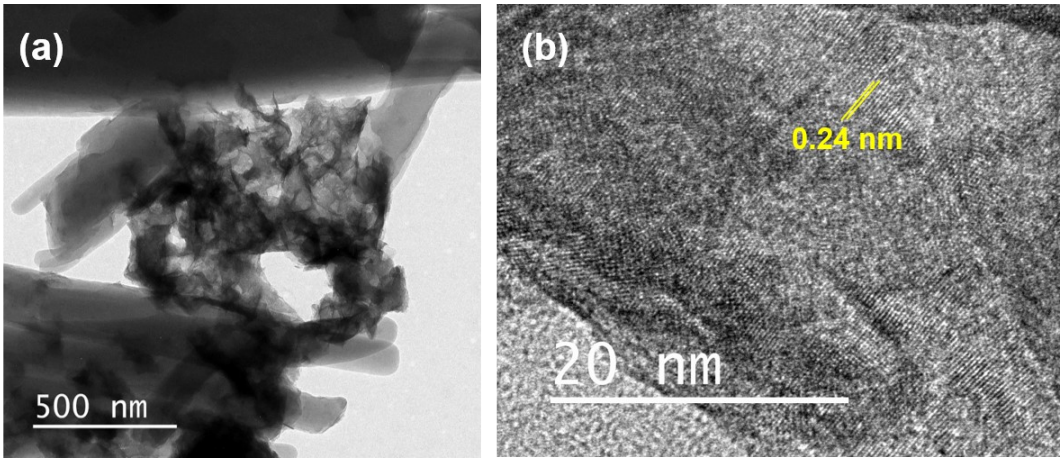

Figure S23. (a) TEM image of **4** after catalysis; and (b) HR-TEM image of **4** showing d-spacing of 0.24 nm, corresponding to (101) plane of γ-Ni(O)OH phase.

References

1 H.-R. Wen, S.-J. Liu, X.-R. Xie, J. Bao, C.-M. Liu and J.-L. Chen, *Inorg. Chim. Acta*, 2015, **435**, 274–282.
2 B. Singh, *Dalton Trans.*, 2024, **53**, 15390–15402.
3 S. Gupta, P. Arora, Z. Aghaei, B. Singh, T. A. Jackson and A. Draksharapu, *J. Am. Chem. Soc.*, 2025, **147**, 619–626.
4 X. Li, X. Chu, K. Ying, X. Cheng, P. Sun, H. Xu, L. Li, J. Zhang and W. Li, *Inorg. Chem. Front.*, 2025, **12**, 5198–5205.
5 S. Banerjee, N. Awasthi, A. Roychowdhury, D. Samanta, P. Arora, N. Dutta, A. Draksharapu, E. Garribba and S. P. Rath, *Inorg. Chem.*, 2025, **64**, 5431–5441.
6 J. Lee, D. Heo, W. Lee and J. Seo, *J. Am. Chem. Soc.*, 2025, **147**, 14997–15005.
7 B. Singh, T. Ansari and A. Indra, *ACS Appl. Nano Mater.*, 2024, **7**, 15754–15762.
8 S. K. Pandey, S. Pandey, S. Singh, S. Jaiswal, V. Ganesan and M. K. Bharty, *Langmuir*, 2025, **41**, 22246–22256.
9 X. Wei, H. Xiao, Z. Zhang, P. Han, L. Wang, S. Deng, J. Wang, K. Yin, H. Yang, K. Wu and B. Jiang, *Small*, 2025, e09115; https://doi.org/10.1002/smll.202509115
10 L.-H. Zhang, F. Yu, Y. Shi, F. Li and H. Li, *Chem. Commun.*, 2019, **55**, 6122–6125.
11 R. Chaurasia, M. K. Bharty, P. Nath, P. K. Sonkar, V. Ganesan, B. Maiti, A. Bharti

and R. J. Butcher, *Polyhedron*, 2019, **174**, 114160.
12 Anamika, D. K. Yadav, K. K. Manar, C. L. Yadav, K. Kumar, V. Ganesan, M. G. B. Drew and N. Singh, *Dalton Trans.*, 2020, **49**, 3592–3605.
13 R. Moi, K. Nath, D. Ghosh and K. Biradha, *ChemCatChem*, 2023, **15**, e202300694.
14 S. Choi, S.-J. Kim, S. Han, J. Wang, J. Kim, B. Koo, A. A. Ryabin, S. Kunze, H. Hyun, J. Han, S.-C. Haw, K. H. Chae, C. H. Choi, H. Kim and J. Lim, *ACS Catal.*, 2024, **14**, 15096–15107.
15 M. Gao, W. Sheng, Z. Zhuang, Q. Fang, S. Gu, J. Jiang and Y. Yan, *J. Am. Chem. Soc.*, 2014, **136**, 7077–7084.
16 S. Kumar Pal, B. Singh, J. K. Yadav, C. L. Yadav, M. G. B. Drew, N. Singh, A. Indra and K. Kumar, *Dalton Trans.*, 2022, **51**, 13003–13014.
17 N. Kamboj and R. K. Metre, *Inorg. Chem.*, 2024, **63**, 9771–9785.
18 R. Chaurasia, S. K. Pandey, D. K. Singh, M. K. Bharty, V. Ganesan, S. K. Hira, P. P. Manna, A. Bharti and R. J. Butcher, *Dalton Trans.*, 2021, **50**, 14362–14373.
19 J. Masud, P.-C. Ioannou, N. Levesanos, P. Kyritsis and M. Nath, *ChemSusChem*, 2016, **9**, 3128–3132.
20 J. A. Bharatbhai, S. Roy, A. Dey, T. Aziz, S. Tothadi, M. Bandhyopadhyay, S. Giri and S. Das, *Small*, 2025, **21**, 2504175.
21 L. Trotochaud, S. L. Young, J. K. Ranney and S. W. Boettcher, *J. Am. Chem. Soc.*, 2014, **136**, 6744–6753.
22 S. K. Pal, T. Ansari, C. L. Yadav, N. Singh, P. Lama, A. Indra and K. Kumar, *Dalton Trans.*, 2025, **54**, 1597–1609.
23 B. Singh, S. Verma, P. Mannu, T. H. Binh, C. L. Dong and A. Draksharapu, *Angew. Chem. Int. Ed.*, 2025, **64**, e202512246.
24 S. Singha Roy, R. K. Sharma, A. Karmakar, S. Nagappan, B. Pathak and S. Kundu, *Appl. Catal. B Environ. Energy*, 2025, **371**, 125227.
25 P. Nayak, A. K. Singh, M. Nayak, S. Kar, K. Sahu, K. Meena, D. Topwal, A. Indra and S. Kar, *Dalton Trans.*, 2024, **53**, 14922–14932.